

Article

Effect of EDM and Femtosecond-Laser Groove-Texture Collision Frequency on Tribological Properties of 0Cr17Ni7Al Stainless Steel

Liguang Yang ^{1,2}, Wensuo Ma ^{1,*} , Fei Gao ^{2,3} and Shiping Xi ²

¹ School of Mechatronics Engineering, Henan University of Science and Technology, Luoyang 471023, China; bmzgedu@126.com

² Luoyang Bearing Research Institute Co., Ltd., Luoyang 471039, China; 13698807332@126.com (F.G.); yejinxsp@163.com (S.X.)

³ School of Mechanical Engineering, Tsinghua University, Beijing 100084, China

* Correspondence: mawensuo@haust.edu.cn

Abstract: Electric spark and femtosecond-laser surface texture are very effective in antifriction systems, but there are few applications and studies in dry friction. In this study, a groove texture was prepared on the surface of 0Cr17Ni7Al stainless steel via electric spark and femtosecond laser, respectively. The tribological properties of the two groove textures under different collision frequencies with the groove were studied under the condition of dry friction. The results show that the friction coefficient of the groove texture prepared by EDM and femtosecond laser is lower than that of the untextured surface. However, this does not mean that every groove-texture design will reduce wear rate. In addition, the groove texture seems to produce different tribological properties under different preparation methods. It is found that in the friction process of the same load, time and linear velocity, different collision frequencies will affect the friction and wear properties of the surface.

Keywords: collision frequency; electric spark; femtosecond laser; groove texture; tribology



Citation: Yang, L.; Ma, W.; Gao, F.; Xi, S. Effect of EDM and Femtosecond-Laser Groove-Texture Collision Frequency on Tribological Properties of 0Cr17Ni7Al Stainless Steel. *Coatings* **2022**, *12*, 611. <https://doi.org/10.3390/coatings12050611>

Academic Editor: Giorgos Skordaris

Received: 6 April 2022

Accepted: 28 April 2022

Published: 30 April 2022

Publisher's Note: MDPI stays neutral with regard to jurisdictional claims in published maps and institutional affiliations.



Copyright: © 2022 by the authors. Licensee MDPI, Basel, Switzerland. This article is an open access article distributed under the terms and conditions of the Creative Commons Attribution (CC BY) license (<https://creativecommons.org/licenses/by/4.0/>).

1. Introduction

As we all know, the friction and wear between the contact surfaces of mechanical parts directly affect the reliability of the entire equipment or system. Friction and wear directly cause huge economic losses every year. With the improvement of tribological characteristics of mechanical systems, the surface-morphology design of mechanical support has become a relatively weak link in the tribological design of the system. In recent years, based on the lubrication and wear-reduction mechanism under different working conditions [1–3], bionic surface texture has been proven to effectively improve the lubrication performance of the friction pair surface and reduce friction and wear. It then becomes an effective lubrication and wear-reduction method [4–6]. It breaks the traditional view that the smoother the surface, the smaller the friction coefficient will be.

In addition, with the continuous development of the research on the influence of texture on friction and wear properties, there are more and more texture-processing methods, such as machining technology [7], laser-processing technology [8], chemical-etching technology [9], EDM technology [10], shot-peening technology [11], ultrasonic-machining technology [12], electrochemical-machining technology [13,14], etc. It meets the processing needs of different materials, different morphologies, complex textures and surface textures of various friction pairs, as well as promotes the research of texture lubrication and wear reduction. These method has made scholars' research on bionics gradually become a hot topic. Surface texture has been widely extended to the machinery industry, such as bearings [15,16], seals [17], cutters [18,19], drill bits [20], cylinder liner piston rings [21], etc. Texture has become an effective way to achieve high efficiency, miniaturization and high reliability of mechanical equipment [22].

Recent years, surface texture has become an effective means to improve the tribological properties of friction pairs. Scholars continue to refine and deepen the research on surface texture, and have conducted a lot of research in sliding direction [23], lubricating oil [24,25], additives [26], fabric [27], hydrophobicity [28], increasing wear [29], corrosion resistance [30] and drag reduction [31]. However, in practice, no matter how the surface texture is prepared or what texture shape is used, friction and collision with the edge of texture will generally occur between friction pairs in the process of sliding friction. This kind of friction and collision is often ignored in previous studies. There are few studies on the tribological characteristics of surface texture considering the collision frequency in the friction process.

In this paper, the groove texture of 0Cr17Ni7Al material was prepared by EDM and femtosecond-laser processing. The friction and wear experiments of groove texture were carried out by MFT-5000 friction and wear tester. Under the experimental conditions of the same load, time, linear velocity and different friction radius, combined with the collision frequency of the sliding-friction process, the surface morphology, friction and wear state of the samples were analyzed by three-dimensional white-light interferometer, based on the scanning electron microscope (SEM) and energy-dispersive spectrometer (EDS). Surface tribological properties of groove texture, untexture and two groove-texture preparation methods are compared, in which the friction and wear mechanism is discussed and the tribological properties of the groove-texture surface are studied.

2. Materials and Methods

2.1. Machining Electric Spark Plate

Electric-discharge machining (EDM) uses the electric corrosion phenomenon of positive and negative electrodes during pulse electric discharge to remove excess metal to meet the machining requirements of surface texture [32]. Micro-EDM technology can be used to reverse copy the array of microgroups with a small machining gap. At the same time, because there is no mechanical cutting force between the electrode and the workpiece, it can be added on rigid workpieces such as thin-wall and elastic parts to achieve high machining accuracy. The electrodes used in this experiment were machined; that is, 30 annular arrays with a size of 13.05 mm × 0.7 mm × 0.61 mm processed on the electrode's raised cuboid (as shown in Figure 1). Then, the prepared electrode was used to process the groove texture. The sample of surface texture of electric spark was provided by Luoyang Bearing Research Institute Co., Ltd. the specific parameters of electric-spark equipment are given in Table 1.



Figure 1. Electrode for preparing texture.

Table 1. Specific parameters of electric-spark equipment.

Parameters	Value	Unit
Productivity	500 (max)	mm ³ /min
Processing current	50A (max)	nm
Machining dimension	600 × 400	mm
Total power	9	KVA
Electrode loss	0.1 (max)	%
Surface roughness	0.1	μm

2.2. Processing Femtosecond-Laser Plate

Femtosecond-laser processing (FS) irradiates the laser beam onto the surface of the workpiece. The laser beam interacts with the material. The material-removal mechanism is the vaporization of the matrix material, with almost no heat-affected zone [33], to realize the processes of cutting, welding, surface treatment, drilling and micromachining of materials (including metal and nonmetal). Femtosecond-laser surface-texture samples were provided by Shenzhen transcend laser Intelligent Equipment Co., Ltd. (Shenzhen, China). Table 2 shows the specific parameters of femtosecond-laser equipment.

Table 2. Specific parameters of femtosecond-laser equipment.

Parameters	Value	Unit
Pulse frequency	1–2000	KHz
Laser wavelength	1030	nm
Cutting format	700 × 600	mm
Cutting efficiency	800–7000	mm/s
Laser power	20 (max)	W
Comprehensive accuracy	±30	μm

According to the above two preparation methods, surface grooves with width of 800 μm, depth of 150 μm, length of 12 mm and 30 grooves were processed, as shown in Figures 2 and 3, respectively.

**Figure 2.** Electric-spark texture.

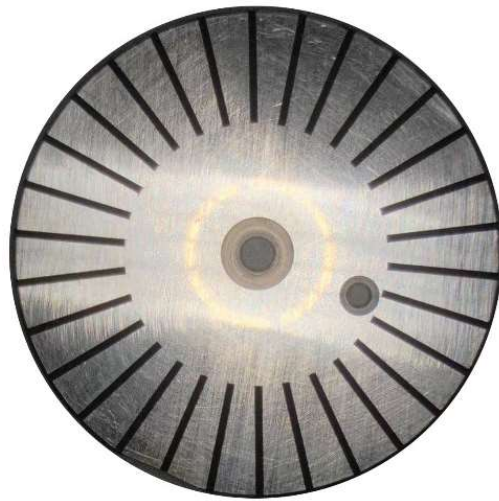


Figure 3. Femtosecond texture.

2.3. Friction and Wear Test Material

The friction characteristics of micromechanical groove texture on 0Cr17Ni7Al surface were experimentally studied using friction and wear testbed (MFT-5000). The testing machine is shown in Figure 4, with the relevant parameters of the test piece shown in Table 3.

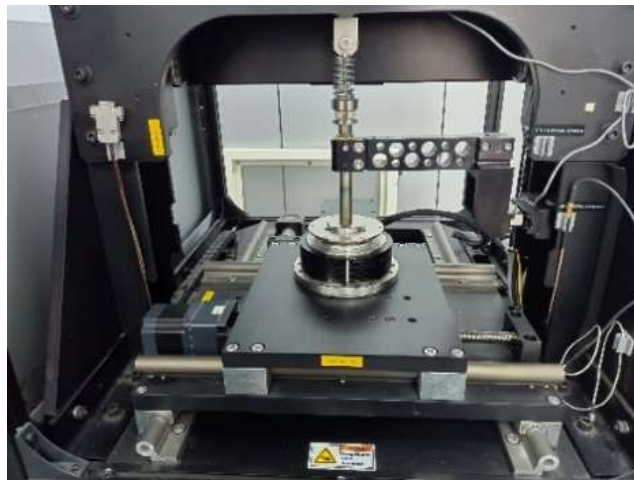


Figure 4. MFT-5000 Friction and wear test bench.

Table 3. Parameters of texture samples.

Test Piece	Geometric Dimension	Hardness	Material	Surface Roughness
Upper test ball	$\Phi 9.525$ mm	64 HRC	9Cr18	$0.014 \mu\text{m}$
Lower test plate	$\Phi 50.8$ mm \times 6.35 mm	42 HRC	0Cr17Ni7Al	$0.05 \mu\text{m}$

The relative position of the friction pair in the friction and wear test is shown in Figure 4. The experimental parameters are shown in Table 4.

Table 4. Experimental conditions for rotation test.

Specimen Name	Test Radius (mm)	Rotation Speed (r/min)	Load (N)	Time (min)
Electric-spark texture	15	60	10	20
	18	50	10	20
	22.5	40	10	20
Femtosecond texture	15	60	10	20
	18	50	10	20
	22.5	40	10	20
Untexture	15	60	10	20
	18	50	10	20
	22.5	40	10	20

Three different test pieces were prepared and compared during the experiment: smooth surface, electric-spark texture and femtosecond-laser texture. Before the test of each sample, acetone was used for further ultrasonic cleaning for 5 min to wipe the surface of the test piece. After the test, the wear morphology was detected by white-light interferometer, scanning electron microscope and energy spectrum. The experimental situation was analyzed combined with the change of friction coefficient.

2.4. Friction and Wear Calculation

The specific experimental parameters are listed in Table 4. The white-light interferometer is used to detect the cross-sectional profile of the wear mark; the wear area is calculated by integrating the cross-sectional profile; and the wear volume is obtained by multiplying the friction step and wear area:

$$W = \frac{V}{F \times S}$$

where W is the wear rate, 10^{-4} mm³/N·mm; V is the wear volume, mm³; F is the normal load, N; S is the running distance, mm. In this study, the error is reduced by the average value of the wear rate of three parallel tests.

3. Results and Discussion

3.1. Friction Coefficient and Wear Rate

It can be seen from Figure 5 that the textured surface can quickly enter the stable wear stage under the same friction conditions. Most of them enter the stable wear stage at 200 s. The groove texture mostly enters the stable wear stage at 200 s. After reaching the stable wear stage, the groove texture can be stabilized in a small variation range. It does not change greatly with the increase in friction time. The friction-coefficient curve of the electric-spark texture decreases with the increase in friction radius. When the radii are 18 mm and 22.5 mm, the friction coefficient is relatively stable in the stable wear stage. The friction coefficient of the femtosecond-laser texture first decreases and then increases with the increase in friction radius. The friction coefficient is relatively stable at the radius of 15 mm and 18 mm. It can be seen that the selection of different processing methods and processing principles needs further consideration when using surface texture to reduce friction. With the progress of friction, the untextured surface is difficult or takes a longer time to enter the stable wear. Regardless of the friction radius, the friction increases with the friction time. At least in the friction process of 1200 s, the friction coefficient increases gradually, and the friction is further intensified.

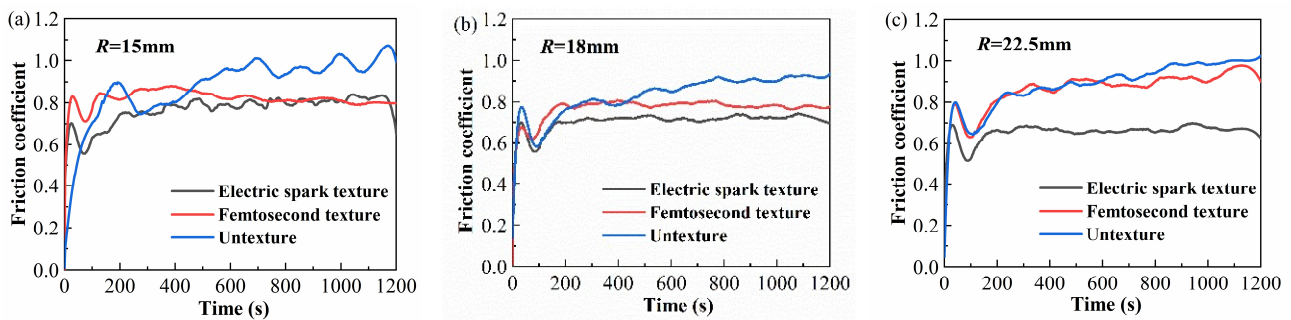


Figure 5. Friction-coefficient curves of different samples: (a) rotation radius 15 mm; (b) rotation radius 18 mm; (c) rotation radius 22.5 mm.

The reason why the friction coefficient of the groove texture is lower than that of the untextured surface may be due to the following three aspects: Firstly, this may be caused by the wear debris on the surface of the groove texture being taken away with friction and captured and stored by the groove texture during the friction process, which reduces the further aggravation of wear particles; Secondly, the ball collides with the groove continuously to result in friction-pair vibration, which makes the wear debris roll and reduces the friction; Thirdly, the existence of texture grooves can reduce the contact area and contact time of the friction pair in the friction process, reduce the increase of friction heat, achieve the effect of heat dissipation, and slow down the formation of oxidative wear and fretting wear. Under the same test conditions, the friction coefficient of the untextured surface increases gradually with the progress of the friction experiment. The main reason is that the wear debris generated in the friction process cannot be discharged in time and also forms three-body wear on the surface of the friction pair, which increases the heat generated by friction and aggravates the wear. Under the same preparation method, the variation of texture friction coefficient with different friction radius may be related to the collision frequency of texture in the friction process. Under different preparation methods, the different variation of texture friction coefficient with friction radius may be related to the influence of different preparation methods on the performance parameters of surface texture.

It can be seen from Figure 6 that the impact frequency has different effects on the groove texture of different preparation methods. The average friction coefficient of the spark texture decreases with the decrease in collision frequency, while the femtosecond texture decreases first and then increases. However, the law of untextured surface is not obvious. It can be seen from Tables 5 and 6 that when the friction radius is 22.5 mm and the collision frequency is 24,000 times, the average friction coefficient of the EDM texture is the minimum $C = 0.6755$. Under the conditions of 15, 18 and 22.5 mm rotation radius, the friction coefficient of the surface modified by electric spark and femtosecond groove texture is less than that of the untextured surface, indicating that the surface texture has good antifriction performance.

As shown in Table 6, under the same sliding linear speed, time and load conditions, the frequency of collision between the upper specimen and the surface groove of the lower specimen is different in the process of friction.

Table 5. Average friction coefficient and wear rate of different samples.

Specimen Name	Rotation Radius (mm)	Average Friction Coefficient	Wear Rate ($10^{-4} \text{ mm}^3/\text{N}\cdot\text{mm}$)
Electric-spark texture	15	0.7686	5.926
	18	0.7149	4.266
	22.5	0.6755	3.662

Table 5. Cont.

Specimen Name	Rotation Radius (mm)	Average Friction Coefficient	Wear Rate ($10^{-4} \text{ mm}^3/\text{N}\cdot\text{mm}$)
Femtosecond texture	15	0.7883	6.82
	18	0.7386	5.031
	22.5	0.8177	3.73
Untexture	15	0.8949	5.219
	18	0.8696	6.352
	22.5	0.8672	5.14

For the wear rate in Figure 7, with the increase in friction radius and the decrease in collision frequency, the electric spark texture and femtosecond texture show a downward trend. When the friction radius is 22.5 mm and the number of collisions is 24,000, the texture wear rate of EDM is the lowest $W = 3.662 \times 10^{-4} \text{ mm}^3/\text{N}\cdot\text{mm}$. The wear rate of femtosecond texture reaches the maximum when the radius is 15 mm and the collision frequency is 36,000 times $W = 6.820 \times 10^{-4} \text{ mm}^3/\text{N}\cdot\text{mm}$.

It can be seen that not all textures of friction radius are more wear-resistant than untextured surfaces. The regularity of the untextured surface is not strong, and it is difficult to predict and judge. The use of friction texture in engineering can not only reduce the wear effect, but also lead to the unreasonable use of friction texture in practice.

Table 6. Collision parameters with different radius of rotation.

Rotation Radius (mm)	Time (min)	Speed (r/min)	Number of Grooves per Turn	Total Number of Friction Turns	Total Times of Friction and Collision
15	20	60	30	1200	36,000
18	20	50	30	1000	30,000
22.5	20	40	30	800	24,000

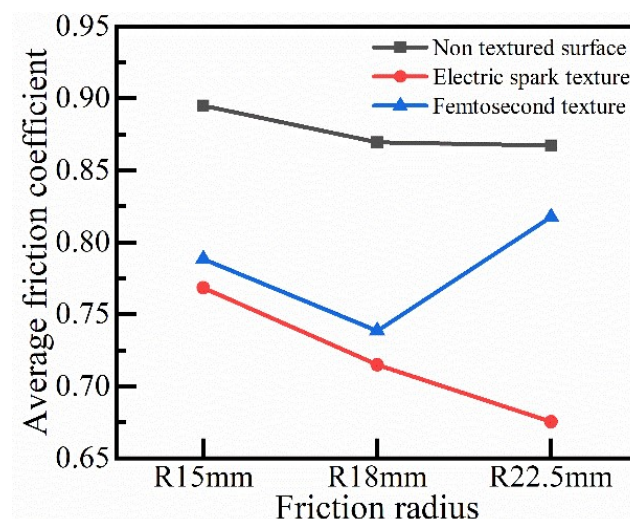


Figure 6. Average friction coefficient of different samples.

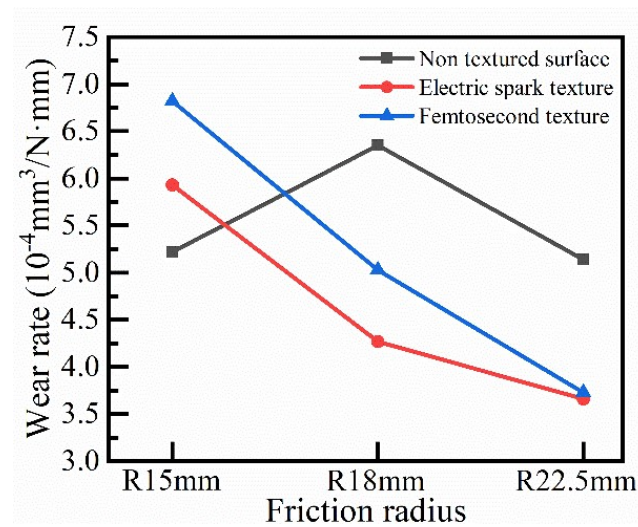


Figure 7. Wear rate of different samples.

3.2. Worn-Morphology Analysis

After the friction experiment, the flaked convex part formed on the surface of the friction pair is called the hard-phase peak [34]. The hard phase peak may be the migration of wear debris under the combined action of load and sliding speed during the friction process. Heat is generated rapidly during friction, and it is cooled rapidly during friction pair collision. Under this repeated action, it is formed by gluing and “cold welding”, which is similar to cold-work hardening. According to the position of hard-phase peak, it can be divided into wear-mark hard-phase peak and wear-mark-edge hard-phase peak.

The hard-phase peak at the edge of the wear mark helps to form a supporting effect on the surface of the friction pair, which could protect the surface from further wear. The hard-phase peak of the wear mark will further aggravate the wear groove effect and even play an important role in the evolution from abrasive wear to adhesive wear.

It can be seen from the three-dimensional wear-trace morphology and wear-trace depth curve in Figure 8 that the hard-phase peak of the untextured surface is basically the hard-phase peak of wear trace under different friction radius. The textured surface is mostly the hard-phase peak at the edge of the wear mark, which is mainly due to the fact that the wear debris on the untextured surface cannot be discharged during the friction process. With the migration of friction, the cemented hard-phase peak is formed at the edge of the wear mark and the wear mark. Most of the wear debris is located in the middle of the wear mark, which is caused by the hard-phase peak of the wear mark being greater than the edge hard-phase peak. During the friction process of the textured surface, the wear debris in the middle of the wear mark, especially the large volume of wear debris, falls into the groove, which greatly reduces the wear debris at the wear mark. The wear debris at the edge of the wear mark failed to migrate far with the friction and was not well-captured by the texture. It remained at the edge of the wear mark and formed the edge hard-phase peak.

The shape of the wear-mark depth curve is concave. The smoother the curve is, the more fully the friction pair is run in. The longer the time to enter the stable stage, combined with the compound effect of the edge hard-phase peak, will help to achieve the optimal antifriction effect. However, the concave part of the wear-mark depth curve is disordered and irregular. The hard-phase peak of the wear mark is convex. The edge hard-phase peak is connected with the hard-phase peak of the wear mark. All these phenomena indicate that the friction is intensifying. It showed that when there are both wear-mark hard-phase peaks and edge hard-phase peaks, the reverse effect of the wear-mark hard-phase peak is much greater than the positive effect of the edge hard-phase peak.

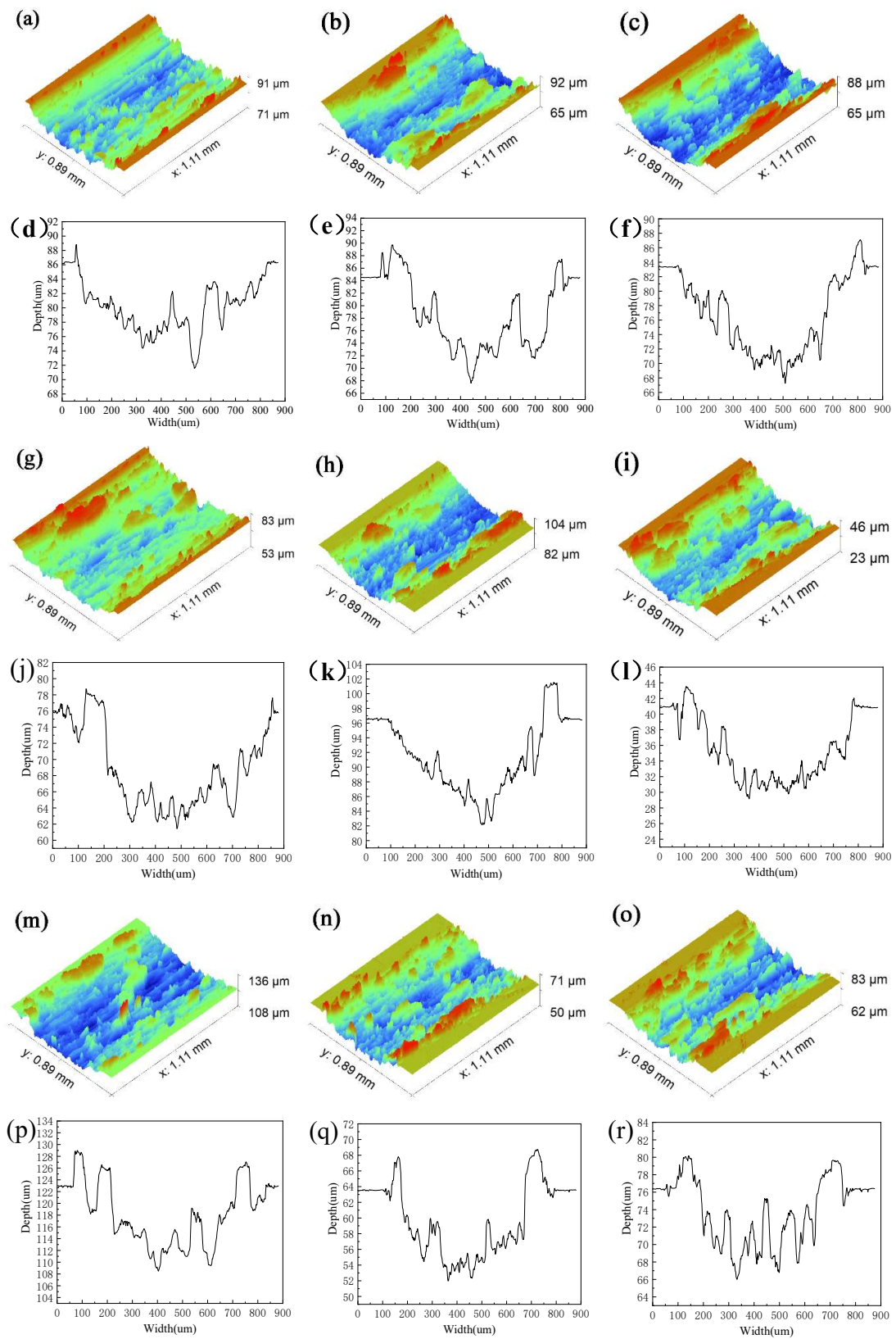


Figure 8. Morphology and depth of wear marks of different samples: (a,d) untexture rotation radius 15 mm; (g,j) untextured rotation radius 18 mm; (m,p) untextured rotation radius 22.5 mm; (b,e) electric-spark texture rotation radius 15 mm; (h,k) electric-spark texture rotation radius 18 mm; (n,q) electric-spark texture rotation radius 22.5 mm; (c,f) femtosecond texture rotation radius 15 mm; (i,l) femtosecond texture rotation radius 18 mm; (o,r) femtosecond texture rotation radius 22.5 mm.

3.3. Scanning Electron Microscope Analysis of the Worn Surface

As shown in Figure 9a–f, a large number of surface spalling has occurred on the untextured surface under any rotation radius. Moreover, there is less wear debris on the surface. However, there are large glued flakes, which are mainly concentrated in the wear-scar area. This is because at the initial stage of wear, abrasive wear is the main form. The wear debris generated by abrasive wear may accumulate and glue together due to the concentrated heat generated at the moment of friction, which will form the hard-phase peak of the wear mark. As mentioned earlier, the hard-phase peak of the wear mark exacerbates further wear. This is also the main reason why the friction coefficient of untextured samples increases gradually and it is difficult to enter stable wear. Under the same test parameters, the wear of the untextured surface is basically the same, which is not affected by the rotation radius.

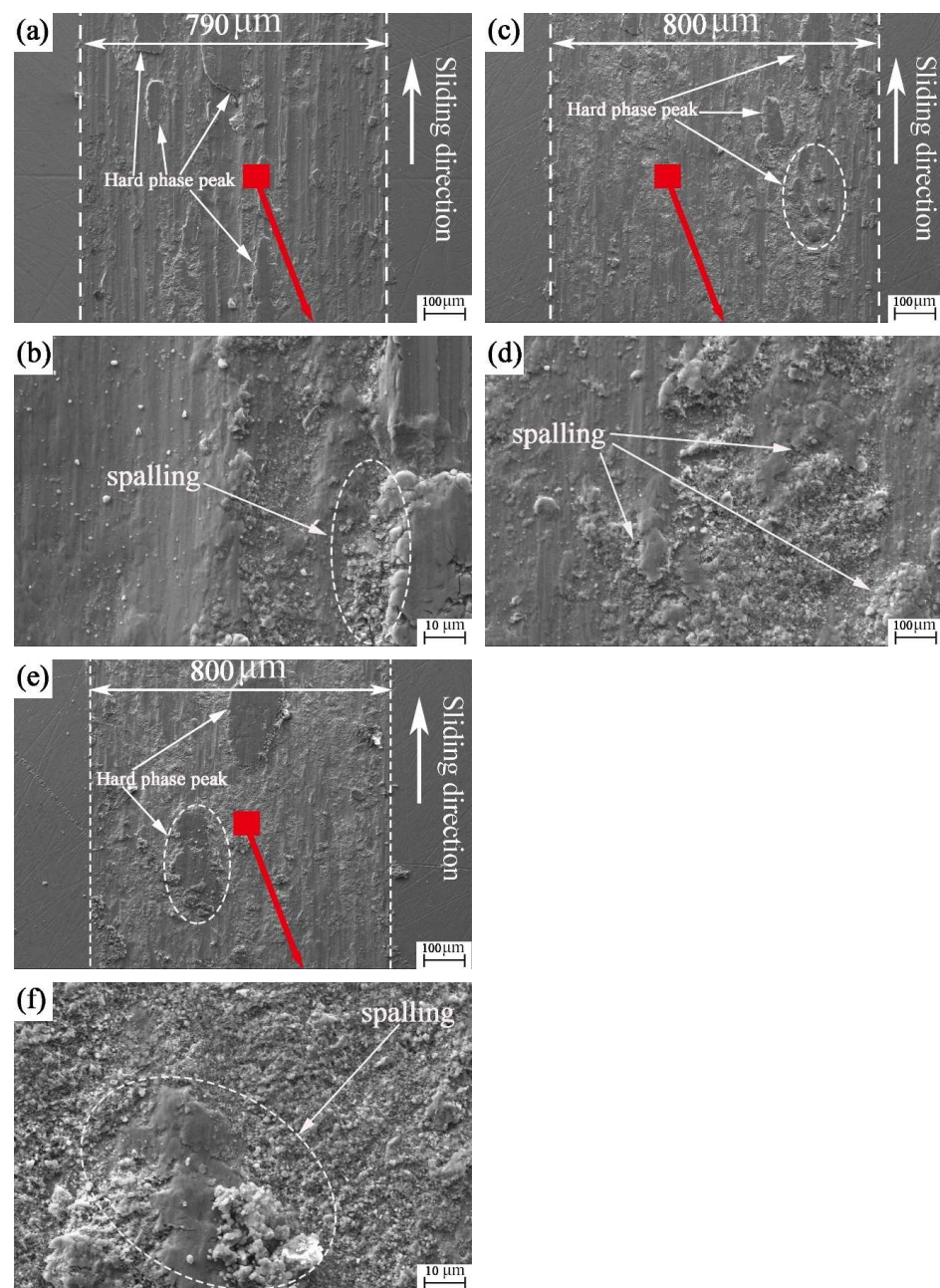


Figure 9. SEM images of the untextured worn plates: (a,b) rotation radius 15 mm; (c,d) rotation radius 18 mm; and (e,f) rotation radius 22.5 mm.

According to the SEM of the ball surface from Figure 10a–i, it can be seen that the wear mark of the ball is round. There are some large particle bulges on the wear-mark surface of the ball, and the wear particles accumulate at the edge of the wear mark along the sliding direction. Moreover, there are several obvious plows in Figure 10e. After the end of friction, these raised abrasive particles and plows can still exist, indicating that these raised abrasive particles have great hardness. It can be inferred that during the friction process, the bulges and plows accumulated by abrasive particles will cut the untextured surface like a sharp edge. Combined with Figure 9, it can be found that the wear marks on both the concave and convex surface of the friction pair are relatively consistent, which further confirms our inference.

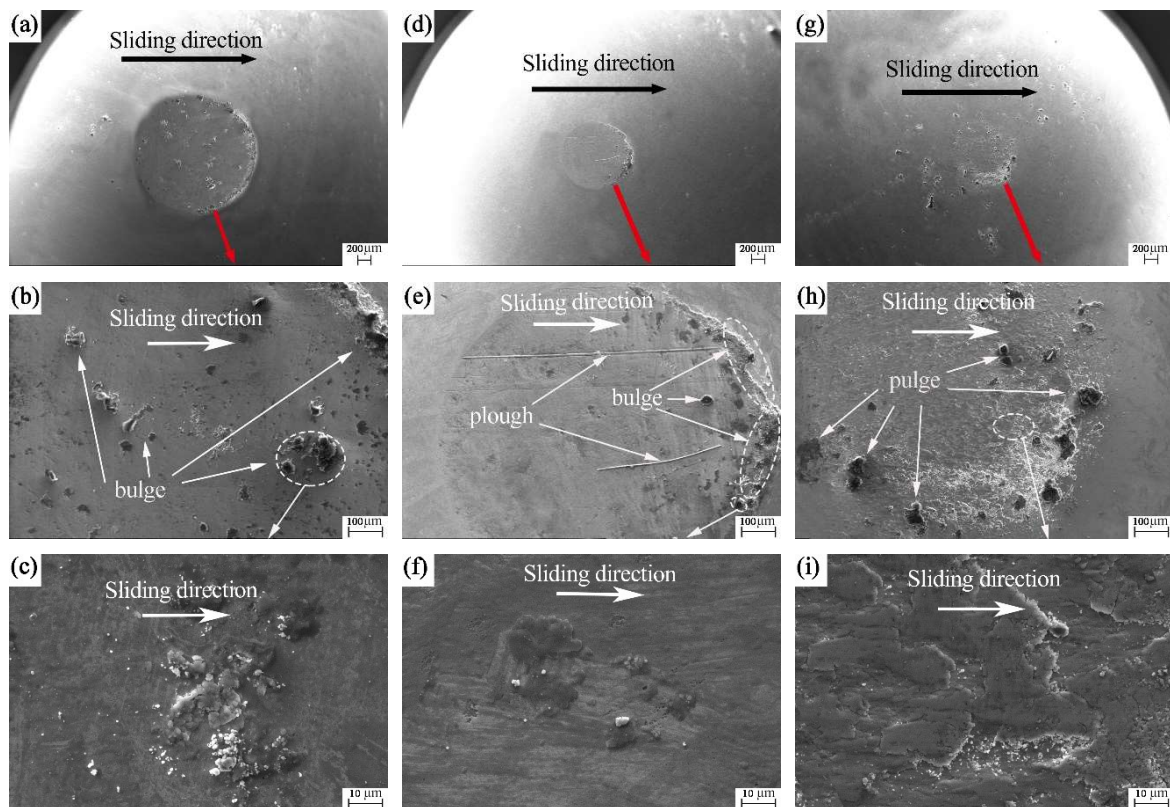


Figure 10. SEM images of the untextured worn balls: (a–c) rotation radius 15 mm; (d–f) rotation radius 18 mm; and (g–i) rotation radius 22.5 mm.

As can be seen from Figure 11a,b, there are many fine-wear debris on the surface of the electric-spark texture. However, no flake cement is found and no hard-phase peak is formed. It shows that the EDM texture is in the stage of abrasive wear. It can be seen from Figure 11c,d that the surface of the EDM texture is still mainly in the form of abrasive wear, with traces of adhesive wear and a few hard-phase peaks of wear marks, but the size is very small and has no obvious impact on wear. As shown in Figure 11e,f, there are both wear debris and flake cement on the surface of the EDM texture. This shows that the surface is in the common development stage of abrasive wear and adhesive wear. The hard-phase peak and edge hard-phase peak of the wear mark are formed at the same time, but the size and number of the edge hard-phase peaks are obviously greater. As mentioned earlier, when two kinds of hard-phase peaks exist at the same time, the positive effect of the edge hard-phase peak is much greater than the reverse effect of the wear-mark hard-phase peak. Thus, the total fusion effect is to reduce friction. It can be judged from Table 6 that with the increase in rotation radius, the collision frequency between ball and groove gradually decreases. The lower the wear rate of the EDM-textured surface, the more obvious the antifriction effect is.

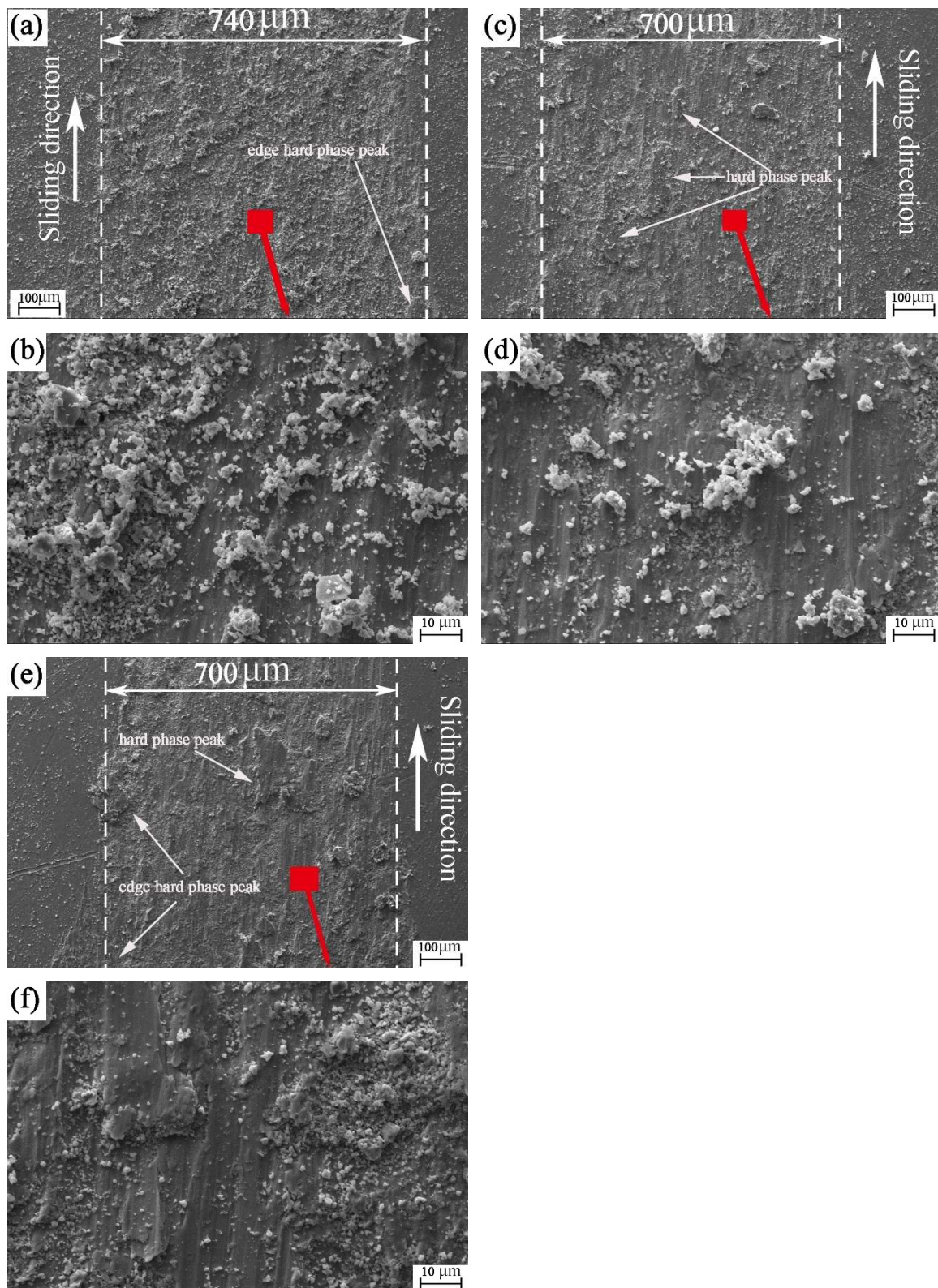


Figure 11. SEM images of the electric-spark-textured worn plates: (a,b) Rotation radius 15 mm; (c,d) Rotation radius 18 mm; and (e,f) Rotation radius 22.5 mm.

According to the SEM of the ball surface from Figure 12a–i, it can be seen that the wear mark of the ball is quadrilateral. The main reason is that during the wear process, the ball collides with the groove and the edge of the groove is equivalent to a sharp edge,

which cuts the wear mark of the ball into a straight line and then becomes a quadrilateral. Figure 12a,d,g shows that the wear marks appear like waves along the sliding direction one by one. This may be because the ball will encounter 30 collisions with the groove texture for each revolution during the friction process. Under the combined action of pressure, speed in the moving direction and friction heat, the wear debris is impact-glued on the wear-mark surface of the ball. In the friction process, such layered waves will achieve the same effect as windsurfing on the sea, which is conducive to reducing the resistance on the surface of the friction pair and alleviating the increasing wear.

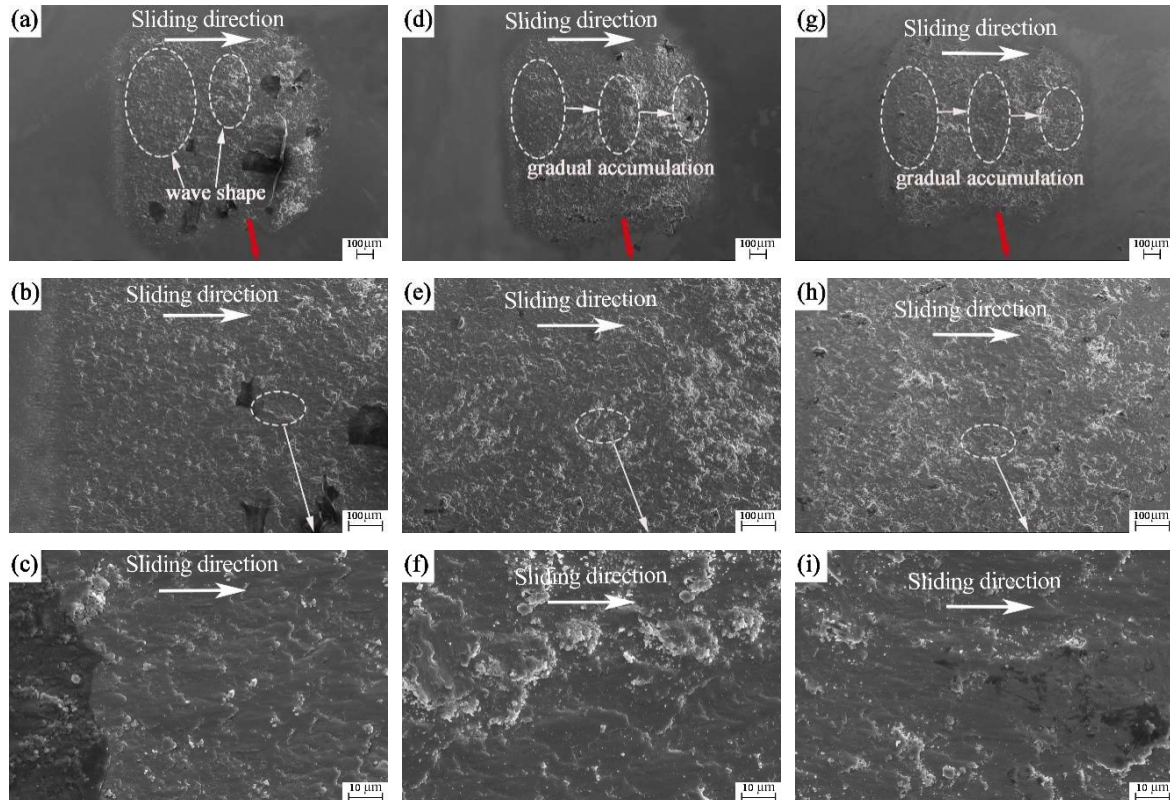


Figure 12. SEM images of the electric-spark-textured worn balls: (a–c) rotation radius 15 mm; (d–f) rotation radius 18 mm; and (g–i) rotation radius 22.5 mm.

As can be seen from Figure 13a–f, there are both wear debris and flake cement on the surface of the femtosecond texture, indicating that the surface of the femtosecond texture is in the common development stage of abrasive wear and adhesive wear. The lamellar glues (hard-phase peaks) are distributed from the edge of the wear mark to the wear-mark area. It can be seen from Figure 13a,b that the size and number of wear-mark hard-phase peaks on the femtosecond texture surface are larger than those on the edge. The two hard-phase peaks are separated from each other, with a long distance and no interaction. At this time, the hard-phase peak of the wear mark plays a decisive role and the wear is intensified. From Figure 13c,d, it can be seen that the hard-phase peak of the wear mark is close to the edge hard-phase peak, which affects each other and roughly offsets the effect. As shown in Figure 13e,f, two kinds of hard-phase peaks have formed a corridor of hard-phase peaks, which interact with each other. The edge hard-phase peak has greater advantages. At this time, the antifriction effect is the main effect.

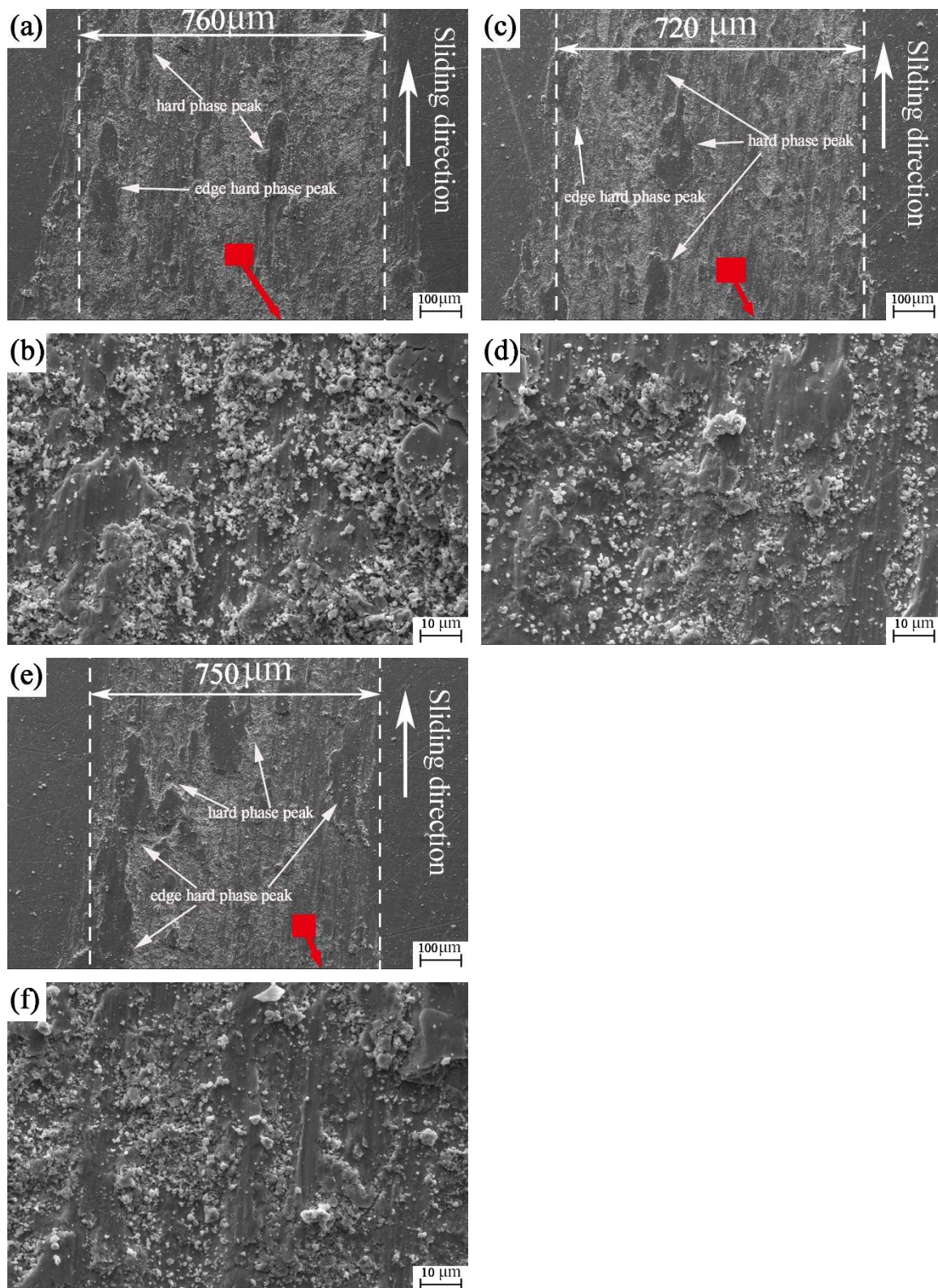


Figure 13. SEM images of the femtosecond-textured worn plates: (a,b) Rotation radius 15 mm; (c,d) Rotation radius 18 mm; and (e,f) Rotation radius 22.5 mm.

According to the SEM of the ball surface from Figure 14a–i, it can be seen that the wear mark of the ball is quadrilateral. The main reason is that during the wear process, the ball collides with the groove and the edge of the groove is equivalent to a sharp edge,

which cuts the wear mark of the ball into a straight line and then becomes a quadrilateral. Figure 14a,d,g shows that the wear marks appear like waves along the sliding direction one by one. This may be because during the friction process, the ball will encounter 30 collisions with the groove texture for each revolution. As mentioned earlier, under the joint action of pressure, speed in the direction of motion and friction heat, the wear debris is impact-glued on the wear-mark surface of the ball. In the friction process, such layered waves will achieve the same effect as windsurfing on the sea, which is conducive to reducing resistance between friction pairs and alleviating the increasing wear. It can be found in Figure 14d that there are abrasive bulges in the ball-milling marks. In the process of friction, it will have a certain impact on the femtosecond texture. However, this bulge is flaked and has little impact.

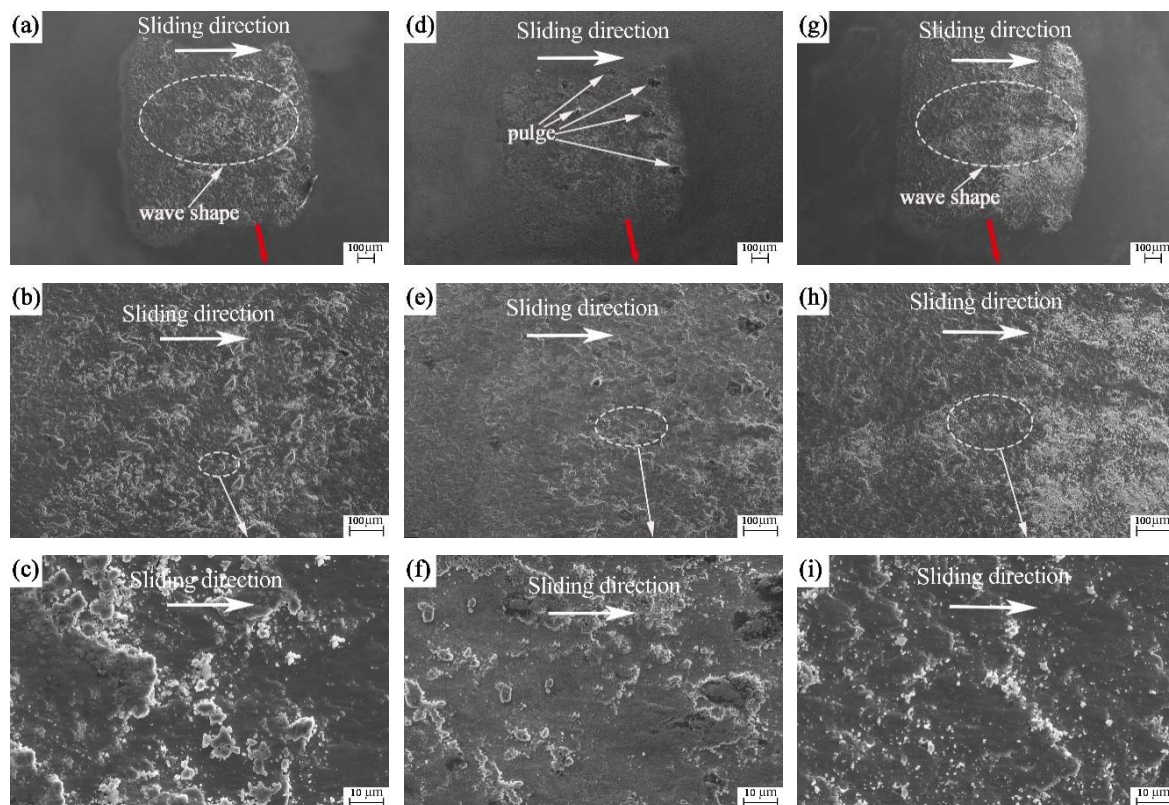


Figure 14. SEM images of the femtosecond-textured worn balls: (a–c) rotation radius 15 mm; (d–f) rotation radius 18 mm; and (g–i) rotation radius 22.5 mm.

From Figure 15a–l, it can be found that the bottom of the groove with electric-spark texture presents the wavy corrosion layer left after electrode discharge. The remelting layer left after femtosecond-laser processing is granular. The groove hardness of both EDM texture and femtosecond texture is higher than that of the original material. The grooves all play good roles in capturing and storing wear debris. As shown in Figure 15a,c,e,g,i,k, there are obvious marks of collision and cutting between the ball and the groove at the edge of the groove, which further confirms our judgment that the quadrilateral wear mark of the groove-texture ball is due to the ball being cut by the edge of the groove.

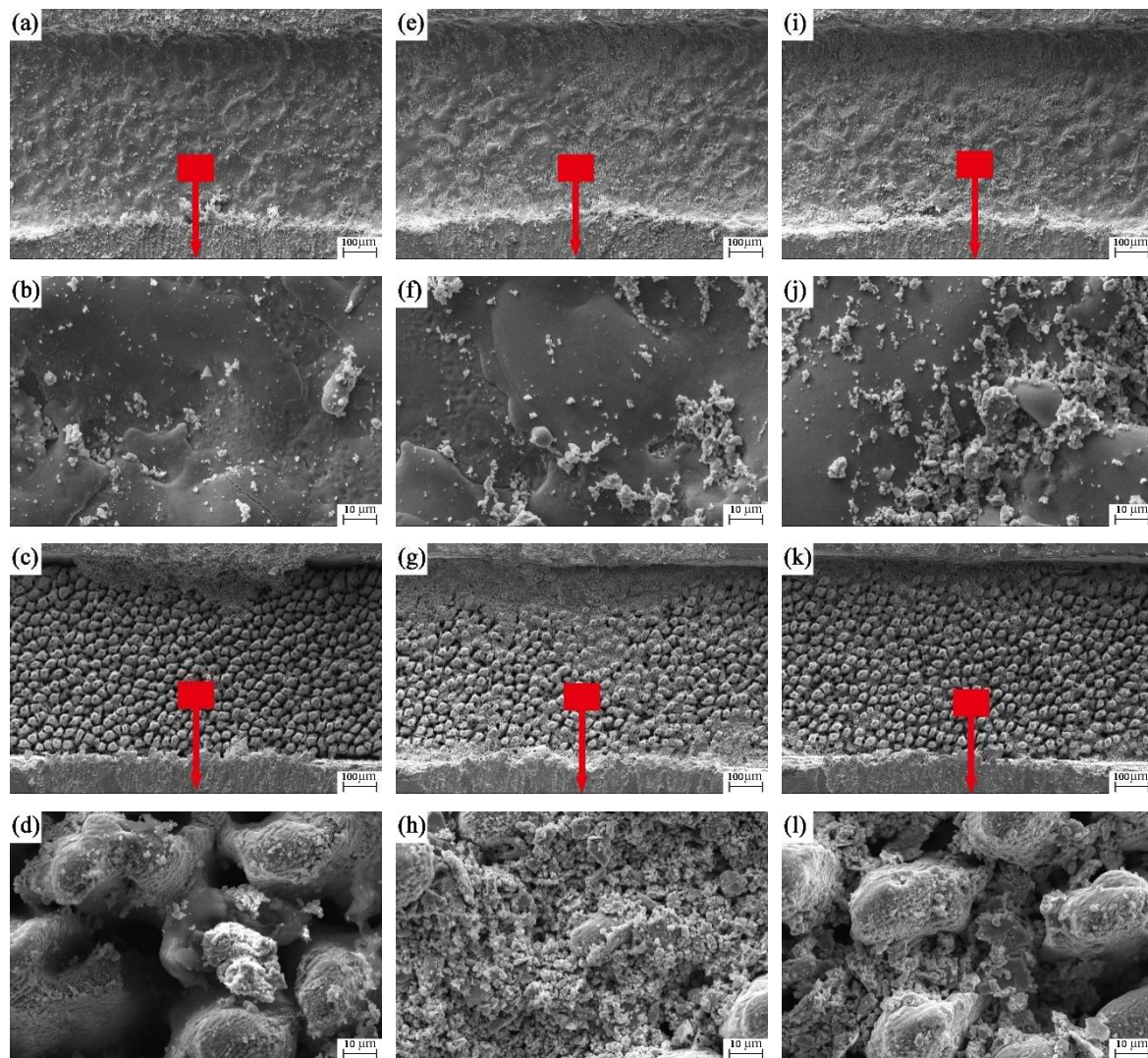


Figure 15. SEM images of the groove-textured worn plates: (a,b) electric-spark texture rotation radius 15 mm; (e,f) electric-spark texture rotation radius 18 mm; (i,j) electric-spark texture rotation radius 22.5 mm; (c,d) femtosecond texture rotation radius 15 mm; (g,h) femtosecond texture rotation radius 18 mm; (k,l) femtosecond texture rotation radius 22.5 mm.

3.4. Energy-Spectrum Analysis of Worn Surface

It can be seen from Table 7 that the chemical composition content of the upper and lower pairs of grinding parts is very similar. Only the content Ni and Al of 0Cr17Ni7Al is higher than that of 9Cr18, so it can be used as a key element. From the energy spectrum of all groups of experiments, the content of the energy-spectrum elements of each surface-modification method under different friction radii is almost the same. Thus, the energy spectrum with radius 15 mm is taken for analysis.

Table 7. Chemical composition and mass fraction of friction pair.

Specimen Name	Material	C	Si	Mn	P	S	Ni	Cr	Al
Plate	0Cr17Ni7Al	0.09	1.0	1.0	0.04	0.03	6.5~7.75	16~18	0.75~1.5
Ball	9Cr18	0.9~1.0	0.8	0.8	0.04	0.03	0.06	17~19	-

According to the energy spectrum in Figure 16a–f, it can be seen that O element is produced in all energy spectra, which proves that there is also oxidation-corrosion wear

in the process of friction besides abrasive wear and adhesive wear that are caused by the action of friction heat and air. It can be seen that there are many kinds of wear forms in the process of this experiment. Comparing the energy spectra of the untextured plate and ball in Figure 16a,b, it is not easy to judge whether the material of the ball has transferred to the disk, but it can be seen from the energy spectrum of the ball that the material of the plate has not transferred to the ball. In Figure 16c,e, no elements of 9Cr18 material were found on the disk surface. It is hard to judge whether the material of the ball has transferred to the plate. However, in Figure 16d,f, in the energy spectrum of the ball, we can see that there is Al element, and the mass fraction of Ni element increases significantly. It can be boldly inferred that the material of the plate with spark texture and femtosecond texture is transferred to the ball. It further confirms our judgment that the wear debris produced by friction is under the joint action of load, sliding friction speed, collision, vibration and friction heat. One part is captured by the groove; another is glued and transferred to the surface of the ball specimen to form corrugated wear marks, which could protect the lower specimen and reduce friction.

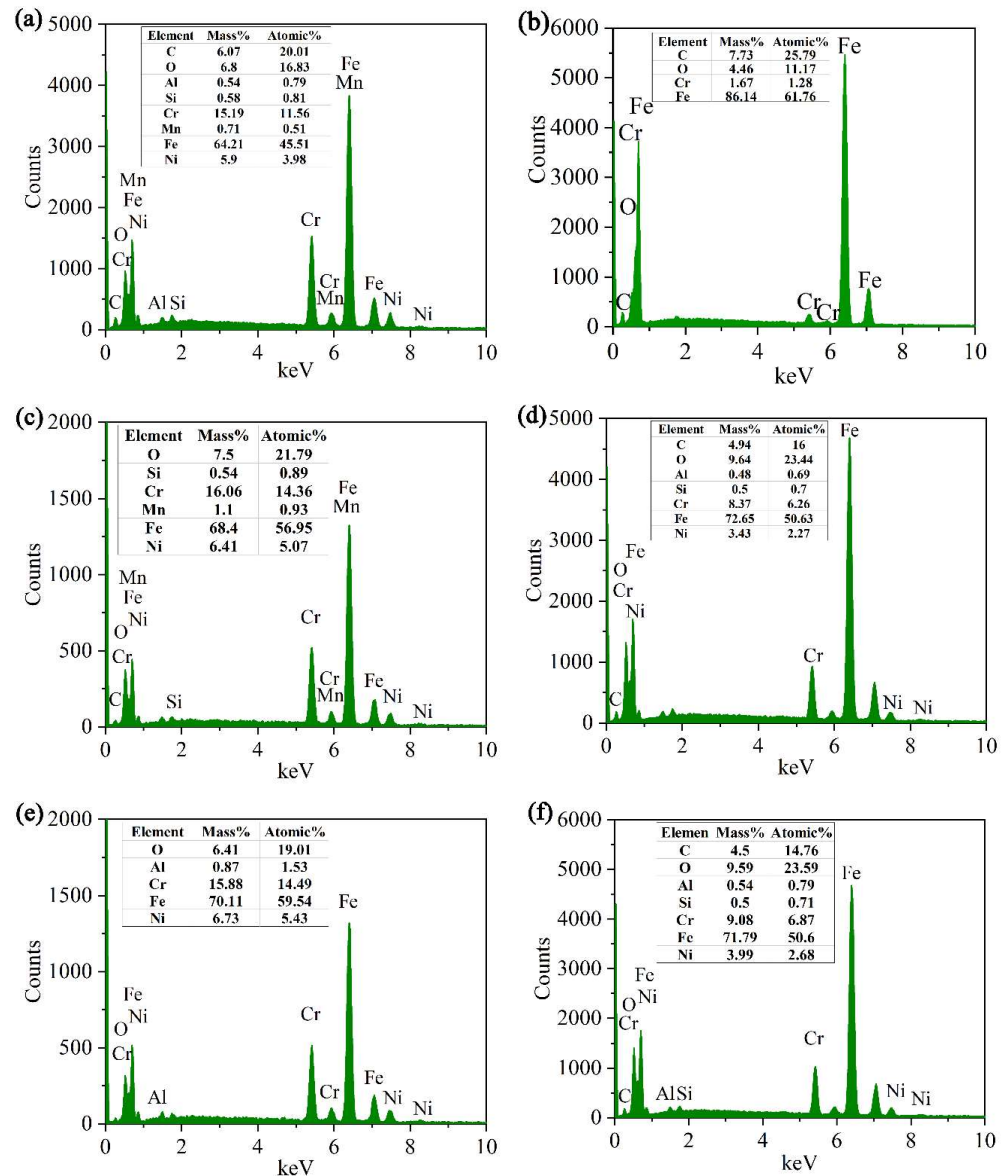


Figure 16. Comparison of EDS spectra of samples used at the rotation radius of 15 mm in the experiment: (a) untextured plate; (b) untextured ball; (c) electric-spark-textured plate; (d) electric-spark-textured ball; (e) femtosecond-textured plate; (f) femtosecond-textured ball.

4. Conclusions

This paper mainly studies the influence mechanism of different groove-collision frequencies on the friction and wear properties of EDM groove texture and femtosecond groove texture on the surface of 0Cr17Ni7Al stainless steel. Some of the main results can be summarized as follows:

(1) The groove texture can be prepared by electric spark and femtosecond laser. The largest friction coefficient of the electric-spark texture and femtosecond texture in the three rotating radii of 15, 18 and 22.5 mm is the friction coefficient of the femtosecond texture at the rotating radius of 22.5 mm $C = 0.8177$. The untextured surface has the lowest friction coefficient $C = 0.8672$. It can be seen that the friction coefficient of both the spark texture and femtosecond texture is significantly lower than that of the untextured surface. However, for the wear rate, not all groove textures are lower than the untextured surface. The wear rate of the femtosecond texture at the rotation radius of 15 mm reached $W = 6.820 \times 10^{-4} \text{ mm}^3/\text{N}\cdot\text{mm}$ which is higher than that under all rotation radii without texture. In addition, the friction coefficient of EDM texture at the rotation radius of 22.5 mm is the lowest $C = 0.6755$. Meanwhile, the wear rate is also the lowest $W = 3.662 \times 10^{-4} \text{ mm}^3/\text{N}\cdot\text{mm}$. The best effect of friction reduction and wear resistance is achieved. Therefore, the choice of preparation method of groove texture is often very important.

(2) In the process of friction, the collision between the ball and groove texture plays a great role. The wear debris changes from sliding friction to rolling friction in order to reduce friction. On one hand, it is conducive to the capture and storage of wear particles by groove texture. On the other hand, the wear debris is moved to the edge of the wear mark, which is more conducive to the formation of the edge hard-phase peak while reducing the formation of the hard-phase peak of the wear mark. The edge hard-phase peak forms a support on the surface of the friction pair to protect the wear-mark area and reduce the wear degree.

(3) The influence of collision frequency on spark texture and femtosecond texture are different. In the experiment, with the increase in rotation radius, the collision frequency decreases from 36,000 to 30,000 to 24,000. The electric-spark texture also shows more and more excellent friction reduction and wear resistance with the decrease in collision frequency. The wear resistance of the femtosecond texture improves with the decrease in collision frequency. However, the friction-reducing performance of the femtosecond texture decreases at the beginning and then increases. It can be seen that for the groove texture, reasonable collision frequency performs better, and not more collision frequency.

(4) It can be seen from the oxygen-element content of the ball in the energy spectrum that there is also oxidative-corrosion wear in the friction process, except abrasive wear and adhesive wear. Al element is added to the energy spectrum of the spherical surface with spark texture and femtosecond texture. The mass content of Ni reached 3.99% and 3.43%, respectively. This is significantly higher than the mass content of the original Ni element on the surface of the ball by 0.06%. The ball collided with the groove texture to transfer and glue wear debris to the surface of the ball-mill mark through the joint action of pressure, rotating speed and friction heat. In this way, a wavy antifriction area was formed, which plays the role of reducing resistance and antifriction.

Author Contributions: Conceptualization, L.Y. and W.M.; methodology, L.Y. and W.M.; software, L.Y.; validation, L.Y., W.M. and F.G.; formal analysis, L.Y. and F.G.; investigation, L.Y. and S.X.; resources, L.Y.; data curation, L.Y. and S.X.; writing—original draft preparation, L.Y. and W.M.; writing—review and editing, L.Y. and W.M.; visualization, L.Y. and S.X.; supervision, L.Y. and S.X.; project administration, L.Y. and S.X.; funding acquisition, L.Y. All authors have read and agreed to the published version of the manuscript.

Funding: This research was supported by the National Key R&D Program of China (Grant No. 2018YFB2000100).

Institutional Review Board Statement: Not applicable.

Informed Consent Statement: Not applicable.

Data Availability Statement: Not applicable.

Conflicts of Interest: The authors declare no conflict of interest.

References

1. Pettersson, U.; Jacobson, S. Textured surfaces in sliding boundary lubricated contacts—Mechanisms, possibilities and limitations. *Tribol.-Mater. Surf. Interfaces* **2013**, *1*, 181–189. [[CrossRef](#)]
2. Kim, B.; Chae, Y.H.; Choi, H.S. Effects of surface texturing on the frictional behavior of cast iron surfaces. *Tribol. Int.* **2014**, *70*, 128–135. [[CrossRef](#)]
3. Shen, X.H.; Tao, G.C. Tribological behaviors of two micro textured surfaces generated by vibrating milling under boundary lubricated sliding. *Int. J. Adv. Manuf. Technol.* **2015**, *79*, 1995–2002. [[CrossRef](#)]
4. Han, J.; Fang, L.; Sun, J.; Ge, S. Hydrodynamic lubrication of microdimple textured surface using three-dimensional CFD. *Tribol. Trans.* **2010**, *53*, 860–870. [[CrossRef](#)]
5. Lu, X.; Khonsari, M.M. An experimental investigation of dimple effect on the stribeck curve of journal bearings. *Tribol. Lett.* **2007**, *27*, 169–176. [[CrossRef](#)]
6. Wang, X.; Liu, W.; Zhou, F.; Zhu, D. Preliminary investigation of the effect of dimple size on friction in line contacts. *Tribol. Int.* **2009**, *42*, 1118–1123. [[CrossRef](#)]
7. Ping, G.; Ehmann, K.F. An analysis of the surface generation mechanics of the elliptical vibration texturing process. *Int. J. Mach. Tools Manuf.* **2013**, *64*, 85–95. [[CrossRef](#)]
8. Tanvir Ahmed, K.M.; Grambow, C.; Kietzig, A. Fabrication of micro/nano structures on metals by femtosecond laser micromachining. *Micromachines* **2014**, *5*, 1219–1253. [[CrossRef](#)]
9. Parreira, J.G.; Gallo, C.A.; Costa, H.L. New advances on maskless electrochemical texturing (MECT) for tribological purposes. *Surf. Coat. Technol.* **2012**, *212*, 1–13. [[CrossRef](#)]
10. Kumar, S.; Singh, R.; Singh, T.P.; Sethi, B.L. Surface modification by electrical discharge machining: A review. *J. Mater. Process. Technol.* **2009**, *209*, 3675–3687. [[CrossRef](#)]
11. Uehara, Y.; Wakuda, M.; Yamauchi, Y.; Kanzaki, S.; Sakaguchi, S. Tribological properties of dimpled silicon nitride under oil lubrication. *J. Eur. Ceram. Soc.* **2004**, *24*, 369–373. [[CrossRef](#)]
12. Fang, S.; Zhao, H.; Zhang, Q. The application status and development trends of ultrasonic machining technology. *J. Mech. Eng.* **2017**, *53*, 22–32. [[CrossRef](#)]
13. Natsu, W.; Ikeda, T.; Kunieda, M. Generating complicated surface with electrolyte jet machining. *Precis. Eng.* **2007**, *31*, 33–39. [[CrossRef](#)]
14. Kern, P.; Veh, J.; Michler, J. New developments in through-mask electrochemical micromachining of titanium. *J. Micromech. Microeng.* **2007**, *17*, 1168. [[CrossRef](#)]
15. Brizmer, V.; Kligerman, Y.; Etsion, I. A laser surface textured parallel thrust bearing. *Tribol. Trans.* **2003**, *46*, 397–403. [[CrossRef](#)]
16. Liu, X.; Dong, L.; Wang, S.; Li, G.; Liu, K. Influence of micro-cavity textured surface on tribological property of grease lubricated spherical bearing. *Tribology* **2014**, *34*, 387–392. [[CrossRef](#)]
17. Dong, H.; Liu, K.; Wang, W.; Liu, X. Laser textured shaft surfaces on the pumping action and frictional properties of lip seals. *Tribology* **2012**, *32*, 126–132. [[CrossRef](#)]
18. Enomoto, T.; Sugihara, T.; Yukinaga, S.; Hirose, K.; Satake, U. Highly wear-resistant cutting tools with textured surfaces in steel cutting. *CIRP Ann.-Manuf. Technol.* **2012**, *61*, 571–574. [[CrossRef](#)]
19. Xi, P.; Cong, Q.; Teng, F.; Guo, H. Design and experiment of bionics pit shape grinding roller for improving wear resistance and crushability. *Trans. Chin. Soc. Agric. Eng.* **2018**, *34*, 55–61. [[CrossRef](#)]
20. Ling, T.D.; Liu, P.; Xiong, S.; Grzina, D.; Cao, J.; Wang, Q.J.; Xia, Z.C.; Talwar, R. Surface texturing of drill bits for adhesion reduction and tool life enhancement. *Tribol. Lett.* **2013**, *52*, 113–122. [[CrossRef](#)]
21. Yin, B.; Lu, Z.; Liu, S.; Fu, Y.; Wang, Y. Theoretical and experimental research on lubrication performance of laser surface texturing cylinder liner. *J. Mech. Eng.* **2012**, *48*, 91–96. [[CrossRef](#)]
22. Bruzzone, A.A.G.; Costa, H.L.; Lonardo, P.M.; Lucca, D.A. Advances in engineered surfaces for functional performance. *CIRP Ann.-Manuf. Technol.* **2008**, *57*, 750–769. [[CrossRef](#)]
23. Saeidi, F.; Meylan, B.; Hoffmann, P.; Wasmer, K. Effect of surface texturing on cast iron reciprocating against steel under starved lubrication conditions: A parametric study. *Wear* **2016**, *348–349*, 17–26. [[CrossRef](#)]
24. Galda, L.; Sep, J.; Olszewski, A.; Zochowski, T. Experimental investigation into surface texture effect on journal bearings performance. *Tribol. Int.* **2019**, *136*, 372–384. [[CrossRef](#)]
25. Liu, C.; Guo, F.; Wong, P.; Li, X. Laser pattern-induced unidirectional lubricant flow for lubrication track replenishment. *Friction* **2021**, *10*, 1234–1244. [[CrossRef](#)]
26. Peng, J.; Shen, M.; Cai, Z. Nano diesel soot particles reduce wear and friction performance using an oil additive on a laser textured surface. *Coatings* **2018**, *8*, 89. [[CrossRef](#)]
27. Qi, X.; Wang, H.; Dong, Y.; Fan, B.; Zhang, W.; Zhang, Y.; Ma, J.; Zhou, Y. Experimental analysis of the effects of laser surface texturing on tribological properties of PTFE/Kevlar fabric composite weave structures. *Tribol. Int.* **2019**, *135*, 104–111. [[CrossRef](#)]

28. Volpe, A.; Covella, S.; Gaudio, C.; Ancona, A. Improving the laser texture strategy to get superhydrophobic aluminum alloy surfaces. *Coatings* **2021**, *11*, 369. [[CrossRef](#)]
29. Pranav, C.; Do, M.T.; Tsai, Y.C. Analysis of high-friction surface texture with respect to friction and wear. *Coatings* **2021**, *11*, 758. [[CrossRef](#)]
30. Wang, Z.; Song, J.; Wang, T.; Wang, H.; Wang, Q. Laser texturing for superwetting titanium alloy and investigation of its erosion resistance. *Coatings* **2021**, *11*, 1547. [[CrossRef](#)]
31. Bai, Q.; Bai, J.; Meng, X.; Ji, C.; Liang, Y. Drag reduction characteristics and flow field analysis of textured surface. *Friction* **2016**, *4*, 11. [[CrossRef](#)]
32. Pham, D.T.; Dimov, S.S.; Bigot, S.; Ivanov, A.; Popov, K. Micro-EDM—Recent developments and research issues. *J. Mater. Process. Technol.* **2004**, *149*, 50–57. [[CrossRef](#)]
33. Chichkov, B.N.; Momma, C.; Nolte, S.; Alvensleben, F.V.; Tünnermann, A. Femtosecond, picosecond and nanosecond laser ablation of solids. *Appl. Phys. A* **1996**, *63*, 109–115. [[CrossRef](#)]
34. Yang, L.; Ma, W.; Gao, F.; Li, J.; Deng, M.; Liu, Z.; Ma, L.; Meng, H. Study on Tribological Properties of groove texture in surface micromachining. *Tool Technol.* **2021**, *55*, 73–76. [[CrossRef](#)]